Crystal Structures of Aspartate Carbamoyltransferase Ligated with Phosphonoacetamide, Malonate, and CTP or ATP at 2.8-Å Resolution and Neutral pH[†,‡]

J. Eric Gouaux, Raymond C. Stevens, and William N. Lipscomb*
Gibbs Chemical Laboratory, Harvard University, Cambridge, Massachusetts 02138
Received March 8, 1990; Revised Manuscript Received May 1, 1990

ABSTRACT: The R-state structures of the ATP and CTP complexes of aspartate carbamoyltransferase ligated with phosphonoacetamide and malonate have been determined at 2.8-Å resolution and neutral pH. These structures were solved by the method of molecular replacement and were refined to crystallographic residuals between 0.167 and 0.182. The triphosphate, the ribose, and the purine and pyrimidine moieties of ATP and CTP interact with similar regions of the allosteric domain of the regulatory dimer. ATP and CTP relatively increase and decrease the size of the allosteric site in the vicinity of the base, respectively. For both CTP and ATP at pH 7, the γ-phosphates are bound to His20 and are also near Lys94, while the α-phosphates interact exclusively with Lys94. The 2′-hydroxyls of both CTP and ATP are near the amino group of Lys60. The pyrimidine ring of CTP makes specific hydrogen bonds at the allosteric site: the NH_2 group donates hydrogen bonds to the main-chain carbonyls of Ile12 and Tyr89 and the pyrimidine ring carbonyl oxygen accepts a hydrogen bond from the amino group of Lys60; the nitrogen at position 3 in the pyrimidine ring is hydrogen bonded to a main-chain NH group of Ile12. The purine ring of ATP also makes numerous interactions with residues at the allosteric site: the purine NH_2 (analogous to the amino group of CTP) donates a hydrogen bond to the main-chain carbonyl oxygen of Ile12, the N3 nitrogen interacts with the amino group of Lys60, and the N1 nitrogen hydrogen bonds to the NH group of Ile12. The binding of CTP and ATP to the allosteric site in the presence of phosphonoacetamide and malonate does not dramatically alter the structure of the allosteric binding site or of the allosteric domain. Nonetheless, in the CTP-ligated structure, the average separation between the catalytic trimers decreases by approximately 0.5 Å, indicating a small shift of the quaternary structure toward the T state. In the CTP- and ATP-ligated R-state structures, the binding and occupancy of phosphonoacetamide and malonate are similar and the structures of the active sites are similar at the current resolution of 2.8 Å.

Aspartate carbamoyltransferase [from *Escherichia coli*, EC 2.1.3.2; for recent reviews, see Allewell (1989), Hervé (1989), Kantrowitz and Lipscomb (1988, 1990), Perutz (1989), and Schachman (1988)] provides an excellent example of an allosteric enzyme for which hypotheses concerning mechanisms of cooperativity can be formulated and tested. Aspartate carbamoyltransferase commits aspartate to the pyrimidine pathway by catalyzing the reaction with carbamoyl phosphate (Jones et al., 1955; Reichard & Hanshoff, 1956). The holoenzyme manifests the quintessential properties of an allosteric enzyme: it shows positive cooperativity toward both substrates, inhibition by CTP, and activation by ATP (Gerhart & Pardee, 1962; Gerhart & Pardee, 1963; Bethell et al., 1968). In addition, UTP and CTP synergistically inhibit the enzyme more than either effector alone (Wild et al., 1989).

Aspartate carbamoyltransferase is composed of three regulatory dimers and two catalytic trimers arranged as shown in Figure 1. The isolated catalytic trimer is catalytically active but exhibits neither cooperativity toward substrates (homotropic cooperativity) nor allosteric inhibition by CTP or activation by ATP (heterotropic cooperativity); the regulatory dimer binds ATP and CTP but possesses no catalytic activity (Gerhart & Schachman, 1965). Three-dimensional structures of the CTP-ligated T[1,2] (T^{ctp}; Kim et al., 1987), the PAM-ligated T (pH 7, T_{pam}; Gouaux & Lipscomb, 1990), the PAM- and malonate-ligated R (pH 7, $R_{pam,mal}$; Gouaux & Lipscomb, 1990), the carbamoyl phosphate ligated and succinate-ligated R ($R_{cp,succ}$; Gouaux & Lipscomb, 1988), and the PALA-ligated R (R_{pala}; Ke et al., 1988) states have been determined and thoroughly refined. These structures illustrate the conformational changes that accompany the T → R transition. The separation of the catalytic trimers increases by 12 Å, and they each rotate by 5° in opposite directions around the 3-fold axis. The distance between the zinc domains of the regulatory dimers increases by about 6 Å, and the regulatory dimers

[†] This work was supported by National Institutes of Health Grant GM06920 (W.N.L.) and a National Institutes of Health postdoctoral fellowship (R.C.S.).

[‡] The coordinates have been submitted to the Brookhaven Protein Data Bank.

[1] T is an abbreviation for tense and is used here to indicate the conformational state of the enzyme that has the unit cell dimensions of $a \approx 122$ Å and $c \approx 142$ Å in the space group $P321$; R, an abbreviation for relaxed, indicates the conformational state of the enzyme that has unit cell dimensions of $a \approx 122$ Å and $c \approx 156$ Å also in the space group $P321$. Functionally, the T form shows low activity and low aspartate affinity while the R form has a high activity and a high affinity for aspartate. See Monod et al. (1965) for a discussion on a theory of allosteric transitions in proteins and for an explanation of the nomenclature.

[2] To signify that a structure contains a ligand bound at the active site, we will add an abbreviation of the ligand name as a subscript to either T or R. Alternatively, if the ligand is bound to the regulatory site, then an abbreviation for that ligand will be added as a superscript. For example, the abbreviation for the R-state enzyme ligated with phosphonoacetamide (PAM), malonate (mal), and CTP would be $R^{ctp}_{pam,mal}$; PALA, *N*-(phosphonoacetyl)-L-aspartate; R_{pala}, PALA-ligated R-state enzyme; $R_{cp,succ}$, carbamoyl phosphate ligated and succinate-ligated R-state enzyme; $R_{pam,mal}$, PAM- and malonate-ligated R-state enzyme; $R^{atp}_{pam,mal}$, complex of the R-state enzyme with PAM, malonate, and ATP.

0006-2960/90/0429-7702$02.50/0 © 1990 American Chemical Society

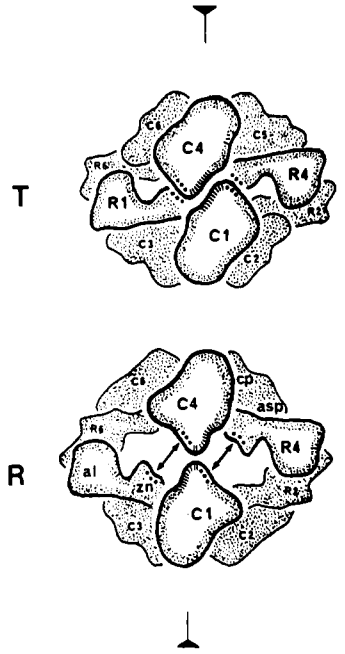

FIGURE 1: Comprising the dodecameric enzyme are two catalytic trimers, each composed of three catalytic chains (C1, C2, C3; C4, C5, C6) and three regulatory dimers, each made up of two regulatory chains (R1, R6; R2, R4; R3, R5); the five oligomers are arranged with approximate D_3 symmetry in the $P321$ crystal forms (Wiley & Lipscomb, 1968). Contained in the asymmetric unit of the $P321$ space group are two catalytic chains, one residing in the upper catalytic trimer and the other in the lower catalytic trimer, and two regulatory chains, comprising one regulatory dimer; the crystallographic 3-fold operation then produces the complete upper and lower catalytic trimers and the two other regulatory dimers. The locations of the carbamoyl phosphate (cp), aspartate (asp), zinc (zn), and allosteric (al) domains are also indicated. The T and R quaternary structures are arranged with the 3-fold axis in the plane of the page and one of the 2-fold axes perpendicular to the plane of the page. As a result of the T to R transition, the separation between the catalytic trimers increases by 12 Å along the 3-fold axis while they rotate 5° in opposite directions around the same axis; each of the three regulatory dimers rotates by 15° about the three 2-fold axes. The asterisks indicate the surface of the enzyme involved in the C1–R4 and C4–R1 interfaces, and the slashes define the regions involved in the C1–C4 contacts. Of particular importance are the differences in these interfaces in the T and the R states.

themselves rotate 15° around the 2-fold axes as illustrated in Figure 1. The detailed structural information revealed from these crystallographic studies has provided the foundation upon which stereochemical mechanisms for the chemical catalysis (Gouaux & Lipscomb, 1987) and the homotropic cooperativity (Ke et al., 1988; Kantrowitz & Lipscomb, 1988; Gouaux et al., 1990) have been devised.

The binding of ATP or CTP to the sites on the regulatory dimers produces opposite effects on the homotropic cooperativity, on the aspartate concentration required to achieve half-maximal velocity (Gerhart & Pardee, 1964), and on the average affinity for PALA (Newell et al., 1989). Unlike the positive cooperativity associated with substrate binding, the binding of the nucleoside triphosphates exhibits negative cooperativity, as shown by Scatchard plots (Buckman, 1970; Gray et al., 1973; Matsumoto & Hammes, 1973; Allewell et al., 1975; Cook & Milne, 1977; Suter & Rosenbusch, 1977). At pH 7, there are three high-affinity sites distributed among the six regulatory chains for CTP ($K \approx 10$ μM) (Suter & Rosenbusch, 1977). The binding of ATP is analogous except that it binds about 10-fold more weakly (Matsumoto & Hammes, 1973). Crystallographic studies performed by Honzatko and Lipscomb (1982a,b) showed that the negative cooperativity exhibited by ATP and CTP is probably caused by indirect interactions between the two binding sites on each regulatory dimer mediated through their N-termini.

The nucleoside triphosphates act upon the enzyme by binding to the same site on the regulatory dimers, as shown by experiments performed in solution (Gerhart & Pardee, 1963, 1964; Changeux et al., 1968; London & Schmidt, 1972, 1974; Thiry & Hervé, 1978; Ladjimi et al., 1985). X-ray crystallographic studies of enzyme and effector complexes determined that the sites were located on the solvent-exposed face of the 10-stranded β-sheet of the allosteric domains (Lipscomb et al., 1975; Monaco et al., 1978; Honzatko & Lipscomb, 1982a,b). However, no experiments have yet elucidated a stereochemical mechanism for the effect of ATP and CTP on the enzyme.

There are several ways in which the crystallographic studies presented here might more effectively reveal the structural basis for the allosteric effects in comparison to previous experiments. First, many of the previous crystallographic works were performed near pH 6.0; at this pH, the enzyme exhibits low activity and low cooperativity (Pastra-Landis et al., 1978). Furthermore, at pH 6.0 the strengths of CTP inhibition and ATP activation are greatly reduced when compared to their effects at higher pH (Kerbiriou & Hervé, 1973; Thiry & Hervé, 1978). For example, the few interactions between the phosphates of CTP and the residues in the allosteric site as seen in the T^{ctp} structure (Kim et al., 1987) are probably consequences of the low pH. The experiments described in this paper were performed at pH 7.0. Second, the earlier studies did not include substrates or substrate analogues (Honzatko & Lipscomb, 1982a,b; Kim et al., 1987; Stevens et al., 1990). In the presence of phosphate, an active-site ligand, the equilibrium between the T and R states favors the T state by 3.3 kcal/mol (Howlett & Schachman, 1977). Addition of ATP or CTP slightly displaces the equilibrium toward the R and T states, respectively (Howlett & Schachman, 1977). In the crystal, we find that ATP and CTP cause small increases and decreases in the separation of the catalytic trimers, respectively. However, to produce significant changes in the population of T- and R-state molecules with the allosteric effectors, subsaturating concentrations of substrates or substrate analogues are required, as shown by solution X-ray scattering experiments (Hervé et al., 1985). In this paper, we describe experiments on the R-state enzyme, ligated with the weakly bound substrate analogues phosphonoacetamide (PAM) and malonate, in the presence of ATP and CTP.

Experimental Procedures

Materials. 4-Morpholineethanesulfonic acid (MES), ethylenediaminetetraacetic acid (EDTA), sodium azide, 2-mercaptoethanol, poly(ethylene glycol) 8000 (PEG-8000), malonate, ATP, and CTP were purchased from Sigma Chemical Co. and were used without further purification. The synthesis of PAM (Figure 2) has been described previously (Gouaux & Lipscomb, 1990). Native aspartate carbamoyltransferase was isolated as described (Nowlan & Kantrowitz, 1985) from the EK1104 strain of *E. coli*, which contained the plasmid pEK2 carrying the entire native *pyr*BI operon, in the laboratory of E. R. Kantrowitz.

Crystal Preparation. The $R_{pam,mal}$ crystals were prepared by dialyzing the enzyme at a concentration of 15 mg/mL against a buffer containing 20 mM PAM, 20 mM malonate, and 3 mM sodium azide where the pH was adjusted to 5.8 with *N*-ethylmorpholine. Hexagonal rods of dimension 0.7 × 0.7 × 1.5 mm grew in 1–2 weeks. The crystals belong to the space group $P321$ and have unit cell dimensions $a = b =$ 122.2 Å and $c = 156.6$ Å. This crystal form is isomorphous

Table I: Data Collection and Reduction Statistics

structure[a]	unit cell (Å)	resolution (Å)	reflections collected	unique reflections	R_{merge}[c]
$R^{ctp}_{pam,mal}$	a = 122.2, c = 155.2	2.8–6.0	56017	22498 (78%)	0.059
$R^{atp}_{pam,mol}$	a = 122.5, c = 156.5	2.8–6.0	63311	23641 (81%)	0.063

[a] The space group for both forms is $P321$, No. 150. [b] In parentheses are the ratios of the number of observed reflections to the theoretical number of reflections possible, multiplied by 100. [c] $R_{merge} = \sum_{hkl}(\sum_i|I - \bar{I}|/\sum_i I)$.

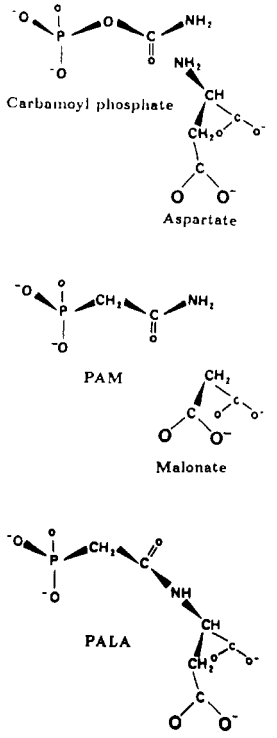

FIGURE 2: Chemical structures of the substrates, carbamoyl phosphate and aspartate, the competitive inhibitors of carbamoyl phosphate and aspartate, phosphonoacetamide and malonate, and the bisubstrate analogue PALA.

to the R_{pala} and $R_{cp,succ}$ forms. After growth, the crystals were transferred to the soaking buffer (30 mM PAM, 15 mM malonate, 2 mM β-mercaptoethanol, 10 mM MES, and 15% PEG-8000 with the pH adjusted to 7 with NaOH). The crystals equilibrated in the soaking buffer for at least 4 days.

The $R^{atp}_{pam,mal}$ crystals were then prepared by making a 10-mL solution of the soaking buffer 10 mM in ATP, pH 7. A small volume of the ATP soaking buffer was placed in a thin-walled silanized glass capillary and a crystal that had been in the soaking buffer was transferred to the capillary and allowed to sink to a position in the capillary suitable for final mounting and data collection. The open end of the capillary was sealed with clay. The crystal soaked in the ATP soaking solution in the capillary for 5 days prior to data collection with one solution change. We found it necessary to soak the crystals in the capillary because, following a soak in the ATP solution, the crystals were very fragile and cracked upon mounting. Since the crystals were soaked in the capillary, the crystals were not touched before data collection and the only manipulations required were the removal of the soaking buffer and the sealing of the capillary with soaking solution and wax. The $R^{ctp}_{pam,mal}$ crystals were prepared in an analogous fashion except that the CTP soaking solution was made 2 mM in CTP at pH 7.

Data Collection, Scaling, and Reduction. The X-ray diffraction data from these two derivatives were collected at the Biotechnology Resource, University of Virginia, on the multiwire area X-ray diffractometer (Sobottka et al., 1984) as previously described (Gouaux & Lipscomb, 1989). The integrated intensities from each data set were corrected for background, polarization, and Lorentz factors and then scaled according to the method of Fox and Holmes (1968) as implemented in the CCP4 program package. Table I summarizes the data collection statistics. Due to crystal size, crystal quality, and time constraints at the data collection facility, X-ray diffraction data for these derivatives were measured to 2.8-Å resolution. The data at higher resolution had an unacceptably low signal to noise ratio.

Table II: Refinement Statistics

structure	total atoms[a]	reflections[b]	R_{factor}[c]	rms_{bond}[d] (Å)	rms_{angle}[d] (deg)
$R^{ctp}_{pam,mal}$	7188	20748	0.167	0.014	3.2
$R^{atp}_{pam,mal}$	7165	21805	0.183	0.017	3.5

[a] Only protein and ligand atoms were included in the refinements. [b] The numbers of reflections used in the refinements with $I \geq 2\sigma(I)$. [c] $R_{factor} = \sum_{hkl}(||F_o| - |F_c||/|F_o|)$. [d] The rms deviations of bond lengths and three atom bond angles from the corresponding parameters contained in version 1.5 of X-PLOR.

Structure Refinement. Both the $R^{ctp}_{pam,mal}$ and $R^{atp}_{pam,mal}$ structures were solved by the molecular replacement method. The initial model for the ATP and CTP structures was the $R_{pam,mal}$ structure (Gouaux & Lipscomb, 1990), which was also determined at pH 7. All refinements were carried out by using the computer program X-PLOR (Brünger, 1989) running on either a Cray YMP at the Pittsburgh Supercomputer Center or a VAX Station 3500. The stereochemical restraints imposed on the structures consisted of the default bond, angle, torsion, improper, and van der Waals energy functions as defined in version 1.5 of X-PLOR. A summary of the refinement is given in Table II. The bond lengths and angles for the zinc–sulfur interactions in the regulatory chain were derived from a crystal structure of a small molecule (Swenson et al., 1978). These values for the zinc–sulfer bond lengths are in agreement with the average values as determined from EXAFS experiments on aspartate carbamoyltransferase (Phillips et al., 1982). We empirically adjusted the force constants on the bond and angle terms for the zinc–sulfur cluster to maintain an approximate tetrahedral geometry. The models for malonate and PAM were generated as previously described (Gouaux & Lipscomb, 1990). The parameters for ATP were extrapolated from the crystal structure of the ATP, manganese, and dipyridylamine complex (Sabat et al., 1985), and the parameters for CTP were determined from a combination of the data from the crystal structure of CMP and the triphosphate parameters from ATP. To prevent the charges on the ligand atoms from biasing the refined structure, we turned off all of the charges on the ligand atoms.

We refined the $R^{ctp}_{pam,mal}$ and $R^{atp}_{pam,mal}$ structures employing the Powell minimization method as incorporated into X-PLOR (Brünger, 1988). However, prior to refinement, we inspected all of the histidine residues in an effort to determine their protonation states on the basis of their hydrogen-bonding environments. Although in some cases the results were ambiguous, frequently an estimate of the protonation state could be made on a chemical basis. In the ambiguous cases, the histidine was defined in the structure and coordinate files as bearing two protons. Throughout the refinements all of the

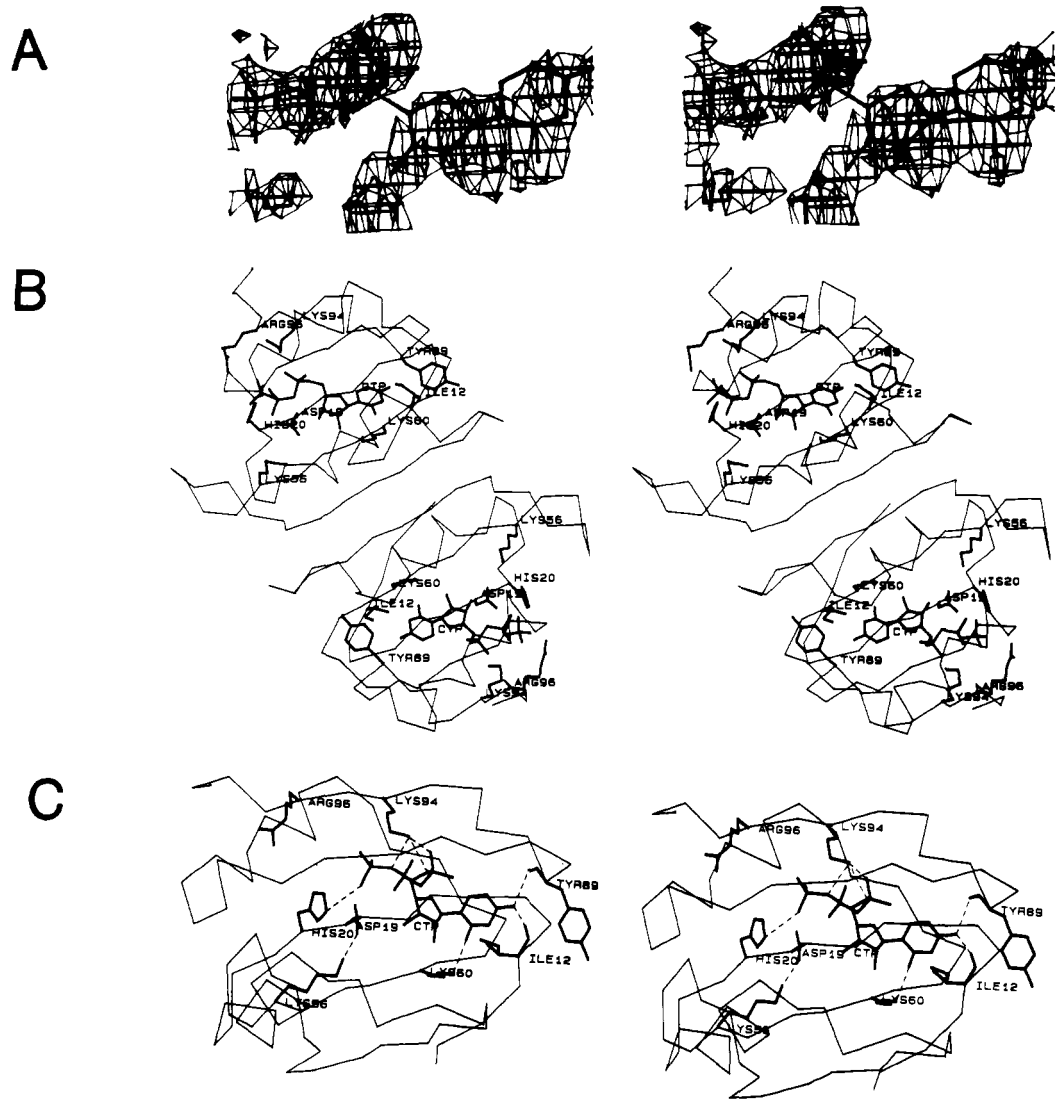

FIGURE 3: (A) $(|F_o| - |F_c|)e^{i\alpha_{calc}}$ electron density for CTP in the R1 chain contoured at 1.8σ. Although the density is not completely continuous, it is clear how to place the base and the triphosphate groups. (B) Stereoview of the location of the CTP binding site in the allosteric domains of the regulatory dimer. CTP (and ATP) bind in a "valley" defined primarily by the N-terminus, the 50s loop, and the loop near residue Tyr89. This view is down the 2-fold axis looking toward the central cavity. Only the α-carbons and some selected side chains are plotted. (C) Close-up of some of the salt links and hydrogen bonds that CTP makes with residues in the R1 active site.

charges on the side-chain groups of the Asp, Glu, Arg, Lys, and His residues were turned off.

Following refinement of the $R^{ctp}_{pam,mal}$ and $R^{atp}_{pam,mal}$ structures to crystallographic residuals of between 0.167 and 0.183, $(|F_o| - |F_c|)e^{i\alpha_{calc}}$ and $(2|F_o| - |F_c|)e^{i\alpha_{calc}}$ maps were calculated, allowing the ligands and a few solvent molecules in the active site to be built into the maps; the fit of the protein atoms to the electron density was also checked at this time. In Figures 3 and 4 we show the electron density for CTP and ATP before the ligands were built into the density and before the ligands were incorporated into the refinement. The coordinates in Figures 3 and 4 are the final refined ligand and protein coordinates. After the ligands were built into their respective electron densities, the refinements were continued until the R_{factor} dropped less than 0.01 for five successive cycles of refinement.

To fit the ligands and solvent and protein atoms to the electron density, we used the computer graphics program FRODO (Jones, 1982) in a somewhat modified form (Pflugrath et al., 1984), running on an Evans and Sutherland PS300 graphics system interfaced to a VAX 11/780 computer. The computer programs SUPERIMP (Honzatko, 1986) and X-PLOR (Brünger, 1988; Kabsch, 1976) were employed to superimpose and perform the subsequent analysis of all of the structures described here.

RESULTS

Crystallization and Crystal Soaking Experiments. The crystals of aspartate carbamoyltransferase ligated with PAM, malonate, and either CTP or ATP which diffracted to the highest resolution were obtained by first growing *P*321 R-state crystals at pH 5.8 in the presence of PAM and malonate and then raising the pH to 7 and diffusing CTP or ATP into the crystals. Without resorting to cross-linking reagents, we found that the maximum concentrations of ATP and CTP that would not crack or disorder the crystals were 10 and 2 mM, respectively. Although cocrystals of PALA and CTP can be grown in the presence of Mg^{2+} (Gouaux and Lipscomb, unpublished), we have not yet pursued the structure determination primarily because the tight binding of PALA at the active site might preclude CTP from altering the structure of the enzyme. Unfortunately, we have not yet succeeded in cocrystallizing the enzyme in the presence of PAM and malonate and the allosteric effectors.

Determination of PAM and Malonate Positions. In the $R^{ctp}_{pam,mal}$ and $R^{atp}_{pam,mal}$ structures the placement of PAM relative

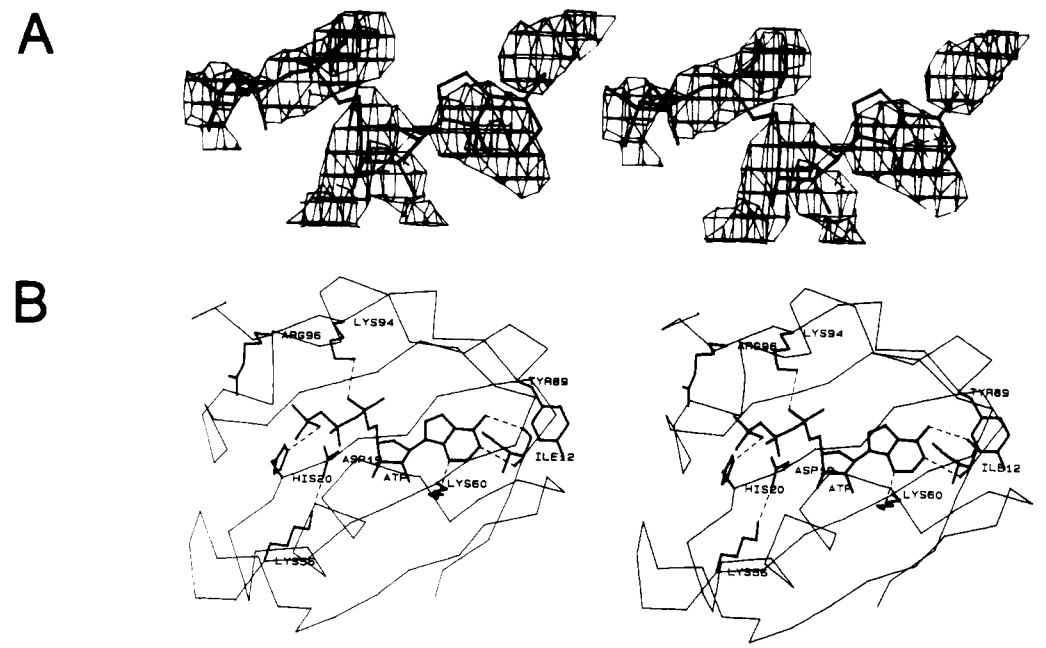

FIGURE 4: (A) $(|F_o| - |F_c|)e^{i\alpha_{calc}}$ electron density for ATP in the R1 chain contoured at 1.6σ. As with CTP, the density is not completely continuous. However, the density for the purine ring is the strongest positive peak in the difference map. (B) Stereoview of the salt links and hydrogen bonds that ATP makes with the residues in the allosteric site.

to the protein atoms was similar to the placement of PAM in the $R_{pam,mal}$ structures (Gouaux & Lipscomb, 1990). Positioning malonate was more straightforward in the $R^{ctp}_{pam,mal}$ and $R^{atp}_{pam,mal}$ structures because the electron density for malonate was stronger, most likely because the concentration of malonate was 2-fold higher. The electron density associated with PAM and malonate in the ATP and CTP structures was calculated as described under Experimental Procedures. After completion of the first stage of refinement, before the ligands were introduced, the electron density peaks corresponding to the phosphonate groups were the strongest peaks in a difference map (8σ) calculated with coefficients $(|F_o| - |F_c|)$ and phases from the refined structure. By comparison of the electron density of PAM and malonate with the electron density associated with a number of well-ordered active-site residues in the ATP- and CTP-ligated structures, it was determined that the occupancies of PAM and malonate in the two structures are similar (approximately 0.6–0.8) at this level of resolution.

Determination of the Positions of ATP and CTP. By use of $(|F_o| - |F_c|)e^{i\alpha_{calc}}$ and $(2|F_o| - |F_c|)e^{i\alpha_{calc}}$ electron density maps calculated after the first stage of refinement, the peaks associated with the bases and the ribose and triphosphate groups for ATP and CTP were located. In both cases, the electron density lobes assigned to the bases were the strongest positive difference peaks (5σ) in the regulatory chains. The electron density associated with CTP and ATP is shown in Figures 3 and 4, respectively. From the locations of the bases, the remaining ribose and triphosphate portions of the nucleoside triphosphates could be readily built into the maps. In the $R^{ctp}_{pam,mal}$ difference maps, there was strong density for CTP in both of the allosteric sites. However, in the $R^{atp}_{pam,mal}$ maps, there was strong density only in the allosteric site of the R1 (B) regulatory chain. Consequently, we built in two molecules of CTP into the $R^{ctp}_{pam,mal}$ structure and one molecule of ATP into the $R^{atp}_{pam,mal}$ structure. CTP and ATP are bound in an anti conformation, similar to their conformations as determined from previous crystallographic studies on nucleoside triphosphates ligated to the T state (Honzatko & Lipscomb, 1982a,b; Kim et al., 1987; Stevens et al., 1990) and from NMR studies (Banerjee et al., 1985). To assess the ligand occupancy at the allosteric sites, we performed a comparison analogous to that made for PAM and malonate in the previous section. This simple test resulted in an estimate of 0.4–0.6 for the occupancy of ATP and CTP with the occupancy of CTP in the R6 chain near the lower value, a result that is similar to the estimated occupancy of CTP in the T^{ctp} structure (Kim et al., 1987).

The electron density associated with CTP and ATP is probably weak for a number of reasons. First, the allosteric domains are the most disordered domains of the structure, as illustrated by their elevated atomic temperature factors (Kim et al., 1988; Ke et al., 1988); one would expect that the disorder in the protein would be transmitted to any associated ligand. Second, the affinity of CTP and ATP for the allosteric site is rather low. Third, the moderate resolution of 2.8 Å intrinsically limits the detail observable in the electron density maps. Nonetheless, we believe that our interpretations of the electron density in the allosteric sites of the $R^{ctp}_{pam,mal}$ and $R^{atp}_{pam,mal}$ structures faithfully describe the binding of the effectors to the enzyme in the crystal. We hope that our results in the crystal can be extended to describe the binding of ATP and CTP to the enzyme in solution. Our results on the binding of ATP and CTP to the R-state enzyme are consistent with previous crystallographic, biochemical, genetic, and NMR experiments. Indeed, the results from the parallel yet independent refinement of the T-state ATP and CTP complexes (Stevens et al., 1990) are in good agreement with the R-state structures. Furthermore, the electron density maps that are shown in Figures 3 and 4 were calculated before the coordinates for CTP or ATP were introduced into the refinement, obviating the possibility of a "memory" effect. Comparison of the electron density maps derived from $R^{ctp}_{pam,mal}$ and $R^{atp}_{pam,mal}$ data sets with maps calculated from the $R_{pam,mal}$ data provides additional evidence for our interpretation of the binding of CTP and ATP.

As is known for other molecules bearing phosphate groups, ATP and CTP binding to the active site can be followed kinetically (Porter et al., 1969) and crystallographically (Honzatko & Lipscomb, 1982a,b). In this study, the concentrations of the active-site ligands PAM and malonate were sufficiently

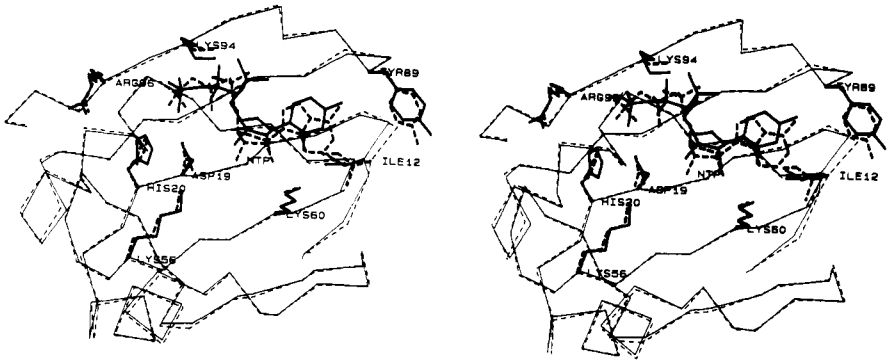

FIGURE 5: Superposition of the $R^{atp}_{pam,mol}$ allosteric domain (R1, unfilled lines) onto the $R^{ctp}_{pam,mal}$ allosteric domain with the application of the transformation also applied to the coordinates of ATP. The largest conformational difference between these two structures is located in the region around Ile12.

high to preclude effector binding to the active site.

Comparison between the Positions of Active-Site Residues and Ligands in the $R^{atp}_{pam,mal}$ and $R^{ctp}_{pam,mal}$ Structures. PAM and malonate interact with the active-site residues of the ATP- and CTP-ligated structure similarly. In fact, PAM and malonate bind to the $R^{ctp}_{pam,mal}$ and $R^{atp}_{pam,mal}$ structures like they bind to the $R_{pam,mal}$ structure (Gouaux & Lipscomb, 1990). The similarity of the interactions between the substrate analogues and the active-site residues in the structure occurs not only because the analogues occupy similar positions but also as a result of the equivalence in positions between the analogous residues in each structure. For example, the overall root mean square (rms) difference in the main-chain atom positions in the $R^{ctp}_{pam,mal}$ and $R^{atp}_{pam,mal}$ structures following superposition of the α-carbons of the C1 chains is 0.2 Å, and the rms deviation in the side-chain positions is 0.36 Å.

Comparison of Interactions between CTP or ATP and the Allosteric-Site Residues. The specific binding of the pyrimidine ring of CTP to the allosteric site is determined by a number of interactions. The hydrogen-bonding interactions consist of bonds between the primary amino group of CTP (N4) and the main-chain carbonyls of Ile12r[3] and Tyr89r, an interaction between the pyrimidine carbonyl oxygen and the amino group of Lys60r, and a hydrogen bond between nitrogen N3 and the main-chain NH group of Ile12r. Near the ribose group are Val9r, Lys60r, Gln84r, and Lys94r. The triphosphate group is bound by polar interactions with Lys94r and His20r, although Lys56r and Arg96r are nearby. The location of the allosteric binding sites on the regulatory dimer and many of the previously mentioned interactions are also illustrated in Figure 3. However, as documented in Table III, some of these interactions occur in only one of the two allosteric sites.

The purine ring of ATP makes three hydrogen bonds to the allosteric-site residues of the R1 (B) regulatory chain. The primary amino group (N10) donates a hydrogen bond to the main-chain carbonyl oxygen of Ile12r, the nitrogen at position 3 is hydrogen bonded to the amino group of Lys60r, and the N1 nitrogen interacts with the main-chain NH group of Ile12r. Interacting with the ribose ring is residue Lys60r and forming hydrogen bonds and salt links to the triphosphate group are Lys94r and His20r. These interactions are summarized in Table IV and illustrated in Figure 4.

As shown in Figure 5, the superposition of the R1 allosteric domain of the $R^{atp}_{pam,mal}$ structure onto the allosteric domain of the $R^{ctp}_{pam,mal}$ structure and the application of the calculated transformation to the coordinates of ATP result in an excellent correspondence between the locations of the triphosphate, the ribose, and the aromatic ring portions of ATP and CTP. In fact, the positions of the primary amino groups are very similar. The carbonyl oxygen of CTP and a purine nitrogen (N3) of ATP also occupy approximately the same positions. Schematic drawings for the binding of CTP and ATP to the allosteric domains are given in Figures 6 and 7, respectively.

Table III: CTP Binding Site Interactions

ligand atom[a]	protein atom[b]	distance[c] (Å)	ligand atom[a]	protein atom[b]	distance[c] (Å)
C_2	Ile12 CG2	3.4/4.7	$O_{2'}$	Val9 CG1	6.5/3.1
O_2	Ala11 CA	5.2/3.4	$O_{2'}$	Val9 O	8.7/3.1
O_2	Ile12 CG2	3.1/4.0	$O_{2'}$	Lys60 NZ	3.5/2.9
O_2	Lys60 NZ	2.8/2.8	$C_{5'}$	Asn84 ND2	3.0/3.4
N_3	Ile12 CG2	3.0/4.5	$C_{5'}$	Lys94 NZ	3.4/7.0
N_3	Ile12 N	3.8/2.7	$O_{5'}$	Val91 CG2	3.1/4.2
N_3	Ala11 C	4.7/3.3	$O_{5'}$	Asn84 ND2	3.0/2.8
N_3	Ala11 CA	5.1/3.0	$O_{5'}$	Lys94 NZ	3.0/5.7
C_4	Ile12 N	4.5/3.5	OPA_2	Lys94 NZ	2.8/3.9
C_4	Ile12 O	3.6/3.4	OPA_2	Lys94 CE	3.9/2.9
N_4	Tyr89 O	3.0/3.6	OPB_3	Lys94 NZ	3.3/5.8
N_4	Tyr89 C	3.4/3.9	OPB_3	Lys94 CE	3.3/5.0
N_4	Tyr89 CA	3.2/3.3	OPG_3	Lys94 CE	3.1/4.4
N_4	Tyr89 CB	3.8/3.5	OPG_3	His20 CE1	4.1/2.9
N_4	Ile12 O	2.8/2.8	OPG_2	His20 CE1	3.0/3.8
N_4	Ile12 N	4.4/3.4	OPG_2	His20 NE2	3.3/3.5
C_6	Val91 CG2	3.5/4.1	OPG_2	Asp19 OD2	3.4/5.1
C_6	Ile86 CD1	3.9/3.5			

[a] The CTP atoms are defined according to the structure given in Figure 3 of Stevens et al. (1990). [b] The protein atom labels are defined according to version 1.5 of X-PLOR (Brünger, 1988). [c] The distance between the atoms in the R1 site is the first number in each pair, and the analogous distance in the R6 site is the second number. An interaction is listed if the ligand to protein atom distance in one of the allosteric sites is less than or equal to 3.5 Å.

Table IV: ATP Binding Site Interactions

ligand atom[a]	protein atom[b]	distance[c] (Å)	ligand atom[a]	protein atom[b]	distance[c] (Å)
N_1	Ile12 N	3.0	N_{10}	Ile12 O	3.2
N_1	Ile12 O	3.4	N_{10}	Tyr89 CA	3.4
N_1	Ile12 CG1	3.0	$O_{2'}$	Lys60 NZ	3.0
C_2	Glu10 O	3.3	OPA_1	Val91 CG2	3.5
C_2	Ile12 N	3.4	OPA_2	Lys94 NZ	3.0
C_2	Ile12 CG1	3.5	OPA_2	Lys94 CE	3.2
C_2	Lys60 NZ	3.4	OPG_2	Asp19 OD2	3.3
N_3	Lys60 NZ	2.9	OPG_2	His20 NE2	3.5
N_3	Lys60 CE	3.4			

[a] The ATP atoms are defined according to the structure given in Figure 3 of Stevens et al. (1990). [b] The protein atom labels are defined according to version of 1.5 of X-PLOR (Brünger, 1988). [c] The distances between ligand and protein atoms in the R1 site that are less than or equal to 3.5 Å.

[3] To differentiate amino acids on the catalytic chains from residues on the regulatory chain, either the specific name of the polypeptide chain will follow the residue name and number or one of the letters c or r will follow, referring to a residue on any of the catalytic or regulatory chains, respectively.

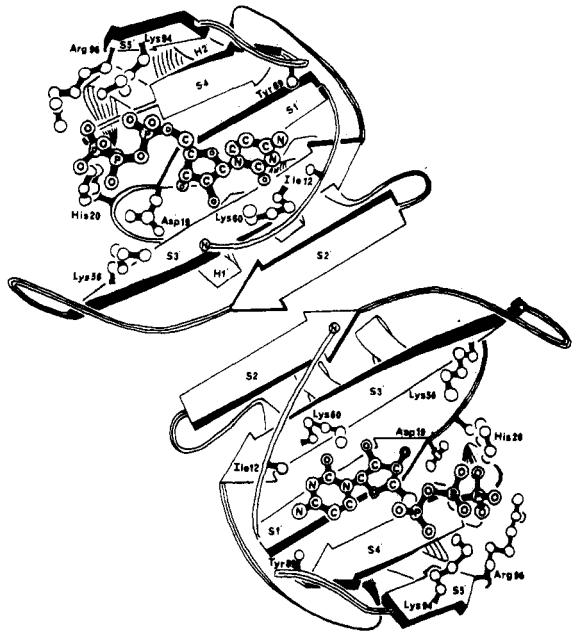

FIGURE 6: Schematic drawing of the binding of CTP to the allosteric domains of the R1 (lower) and R6 (upper) chains of the $R^{ctp}_{pam,mal}$ structure. Some of the residues in contact or near CTP are also shown. The β-strands are drawn as arrows, and the helices, in the background, are depicted as curved arrows.

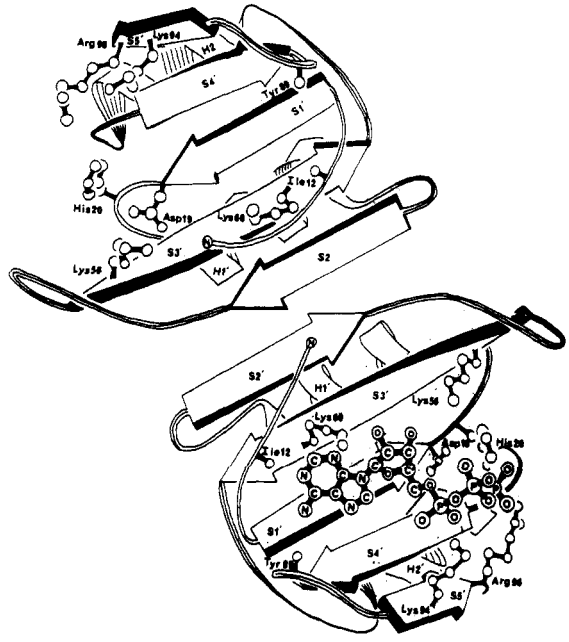

FIGURE 7: Schematic drawing of the binding of ATP to the allosteric domain of the R1 (lower) chain of the $R^{atp}_{pam,mal}$ structure. The R6 site is not sufficiently occupied by ATP to allow the molecule to be built into the map.

Conformational Changes Induced by the Binding of CTP to the $R_{pam,mal}$-Ligated Enzyme. For the $R^{ctp}_{pam,mal}$-ligated enzyme the separation between the catalytic trimers has decreased by ≈0.5 Å from the separation of the trimers in the $R_{pam,mal}$ structure. Accompanying the displacement of the "upper" catalytic trimer relative to the "lower" trimer are movements of the R6 regulatory chain and the allosteric domain of the R1 chain. In addition, the catalytic trimers and regulatory dimers show small rotations (toward the T quaternary structure) about the 3- and 2-fold axes, respectively. However, at the current resolution of 2.8 Å, we find no changes in hydrogen bonds or other polar interactions at the inter- and intrachain interfaces.

Table V: Results of the Superposition of the $R_{pam,mal}$ and $R^{ctp}_{pam,mal}$ Catalytic and Regulatory Chains[a]

initial fit	C1 (Å)	R1 (Å)	R6 (Å)	C6 (Å)
C1	0.20	0.41	0.59	0.54
R1	0.27	0.29	0.55	0.78
R6	0.65	0.45	0.30	0.37
C6	0.45	0.55	0.45	0.19

[a] The α-carbons of each chain of the $R^{ctp}_{pam,mal}$ structure were fit to the corresponding atoms of the $R_{pam,mal}$ structure, and then the rms differences in backbone atom positions between the structures were calculated. Shown in the first row are the rms differences in backbone atom positions for the C1, R1, R6, and C6 chains when the $R^{ctp}_{pam,mal}$ model is superimposed on the $R_{pam,mal}$ structure with the C1 chain as the template. The transformation required to superimpose the C1 chain is also applied to all of the atoms in the molecule. On the remaining rows, the results of using the R1, R6, and C6 chains as templates are given. This procedure is similar to the method employed by Lesk and Chothia (1984) to determine the relative changes in positions of the helices in the "open" and "closed" forms of citrate synthase.

The results of comparisons of the quaternary arrangement of the C1, R1, R6, and C6 polypeptide chains, performed in a fashion analogous to the calculations of Lesk and Chothia on the open and closed forms of citrate synthase (Lesk & Chothia, 1984), are given in Table V. When the C1 chain of the $R^{ctp}_{pam,mal}$ structure is superimposed on the C1 α-carbons of the $R_{pam,mal}$ structure, the rms deviations between the backbone atoms of the C1 chains are lower (0.20 Å) than for the deviations of the C6 chains (0.54 Å). If the C6 chains of the $R^{ctp}_{pam,mal}$ and $R_{pam,mal}$ structures are superimposed, the rms deviation of backbone atoms is 0.19 Å. The transformation from the fit of the C1 chains to the fit of the C6 chains can be described by a translation along the 3-fold axis of ≈0.5 Å. Consequently, the separation of the catalytic trimers has decreased by ≈0.5 Å in the $R^{ctp}_{pam,mal}$ structure in comparison to the $R_{pam,mal}$ and $R^{atp}_{pam,mal}$ structures.

Analysis of the allosteric domains of the R1 and R6 chains indicates that there are no large conformational rearrangements resulting from the ligation of the enzyme with CTP. Instead, there are small shifts in the positions of main-chain and side-chain residues in the binding site and the allosteric domain. Since the differences between the conformations of the allosteric domains of $R_{pam,mal}$ and the $R^{ctp}_{pam,mal}$ structures are on the order of the errors in the coordinates (ca. 0.5 Å, see below), we will focus on those differences that appear to be directly related to the binding of CTP. In the R1 and R6 allosteric sites, residues near the N-terminus relocate to bind to the pyrimidine and ribose rings of CTP. The binding of the triphosphate groups to the R1 and R6 sites probably causes the residues in the regions around His20r, Lys56r, and Lys94r to alter their positions. Residues in both the R1 and R6 chains of the $R^{ctp}_{pam,mal}$ model in the vicinity of Leu66r superimpose with an rms displacement of as much as 0.5 Å onto the $R_{pam,mal}$ allosteric domain, even though these residues are not in direct contact with CTP. However, it is not clear if the binding of CTP produces the local changes at sites distinct from the allosteric pocket or if the differences are due to unexpectedly large errors in the coordinates.

Although there are only small conformational differences between the allosteric domains of the $R^{ctp}_{pam,mal}$ and $R_{pam,mal}$ structures, we nonetheless have found that there are relative movements between the domains. To quantitate these changes, we fit two analogous domains and then determine the transformation required to superimpose a second pair of related domains. Results of calculations such as these are given in Table VI. We find that there is a significant difference in the disposition of the zinc and allosteric domains in the R6 chain of the $R^{ctp}_{pam,mal}$ model when compared to the similar

Table VI: Results of the Superposition of the $R_{pam,mal}$ and $R^{ctp}_{pam,mal}$ Regulatory Chain Domains[a]

initial fit	Zn_1[b] (Å)	All_1[c] (Å)	All_6 (Å)	Zn_6 (Å)
Zn_1	0.19	0.49	0.61	0.52
All_1	0.35	0.31	0.48	0.45
All_6	0.93	0.48	0.31	0.42
Zn_6	0.55	0.61	0.50	0.20

[a] The α-carbons of each domain of the $R^{ctp}_{pam,mal}$ structure were fit to the corresponding atoms of the $R_{pam,mal}$ structure, and then the rms differences in backbone atom positions between the structures were calculated. This table is analogous to Table V. [b] The Zn domain is defined by residues 100–153. [c] The allosteric domain (All) is defined by residues 8–99.

Table VII: Results of the Superposition of the $R_{pam,mal}$ and $R^{atp}_{pam,mal}$ Catalytic and Regulatory Chains[a]

initial fit	C1 (Å)	R1 (Å)	R6 (Å)	C6 (Å)
C1	0.31	0.28	0.36	0.32
R1	0.31	0.28	0.36	0.32
R6	0.25	0.30	0.31	0.26
C6	0.24	0.38	0.34	0.20

[a] The α-carbons of each chain of the $R^{atp}_{pam,mal}$ structure were fit to the corresponding atoms of the $R_{pam,mal}$ structure, and then the rms differences in backbone atom positions between the structures were calculated. This table is analogous to Table V.

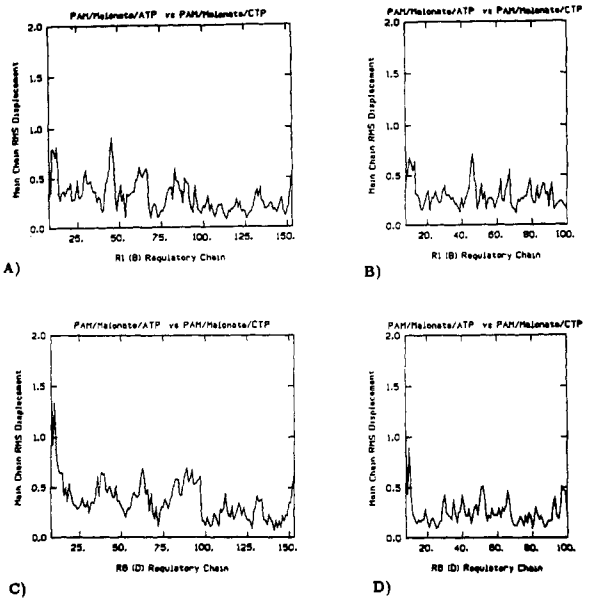

FIGURE 8: (A, C) Fit of the α-carbons of the zinc domains (residues 101–153) of the $R^{atp}_{pam,mol}$ structure onto the analogous atoms of the $R^{ctp}_{pam,mal}$ model for the R1 and R6 chains. (B, D) Superposition of the allosteric domains of the $R^{ctp}_{pam,mal}$ and $R^{atp}_{pam,mal}$ structures for the R1 and R6 chains.

domains of the $R_{pam,mal}$ structure. There is also interdomain movement between the two allosteric domains of the $R^{ctp}_{pam,mal}$ model as defined by a rotation about the vector (–0.67, –0.68, 0.30) of 0.96° and a translation of (–0.22, 0.03, 0.24 Å). The axis of rotation is approximately parallel to the strands of sheet and the helices of the allosteric domains.

Conformational Changes Induced by the Binding of ATP to the $R_{pam,mal}$-Ligated Enzyme. Since ATP only binds with sufficient occupancy to one (R1) of the two allosteric binding sites, we will first consider the conformational changes that occur in this R1 allosteric site. The basis for the comparison will be a superposition of the α-carbons from the allosteric domain of the $R^{atp}_{pam,mal}$ structure on the related regions of the $R_{pam,mal}$ model. Figure 8 displays these results. Analysis of the $R^{atp}_{pam,mal}$ structure using an approach analogous to that employed for the $R^{ctp}_{pam,mal}$ structure indicates that there is no change in the quaternary structure upon ATP binding (Table VII). Nonetheless, there are some local conformational movements. Directly related to the binding of ATP are changes in position of residues near the N-terminus, His20r, the 50rs loop, Tyr89r, and Lys94r. Even though the occupancy for ATP in the other site is very low, some of these differences are also evident in the comparison between the R6 chains. The residues that bind to the triphosphate group have moved slightly from their positions in the $R_{pam,mal}$ structure toward the triphosphate, as noted above for the $R^{ctp}_{pam,mal}$ structure.

In the $R^{atp}_{pam,mal}$ enzyme there are no substantial differences between the relative positions of the domains in the regulatory dimer when compared to the arrangement of the analogous regions of the $R_{pam,mal}$ structure.

Comparison of the Conformational Changes in the $R^{ctp}_{pam,mal}$ and $R^{atp}_{pam,mal}$ Allosteric Sites. In the region around the purine ring of the $R^{atp}_{pam,mal}$ model, the conformational changes are in opposite directions to the changes in the $R^{ctp}_{pam,mal}$ allosteric sites. In order to accommodate the binding of the larger purine ring, the base binding site expands slightly when ATP binds and it contracts from its position in the $R_{pam,mal}$ model when CTP binds, as previously noticed in T-state structures (Honzatko & Lipscomb, 1982a,b). When the allosteric domains from the CTP and ATP R-state structures are superimposed, as shown in Figure 8, the largest differences are at the N-termini and near the 50s loops of the regulatory chains (cf. peak at 45). The difference in the positions of the 50s loops could result from direct binding to the phosphate groups or it might be due to indirect interactions stemming from the distinct positions of the N-termini. This effect could be mediated by the salt link between Glu10R1 and Arg41R1 and then via another side-chain–side-chain interaction between Asp39R1 and Arg55R6.

Experiments are planned to test whether ATP and CTP will actually stabilize the T and the R states of the enzyme, in the *P*321 crystal forms. Since we have shown that the T → R transition can occur within the crystal at neutral pH and at relatively low concentrations of the substrate analogues PAM and malonate, we can determine if ATP and CTP shift the concentration of malonate required to induce the transition to lower and higher concentrations, respectively.

Asymmetry in the Allosteric Domains. Both ATP and CTP occupy the allosteric site in the R1 (B) chain to a greater extent than they bind to the R6 (D) site. Since ATP and CTP were soaked into the crystal and they produce relatively small changes in the allosteric sites in the *P*321 R-state crystals, a preexisting asymmetry in the allosteric sites causes them to both preferentially bind to the R1 site. This might be because the R6 site is a smaller size, which is possibly stabilized by a hydrogen bond between Lys60R6 and the carbonyl oxygen of Val9R6; this interaction is not present in the R1 subsite. There is another violation of the noncrystallographic symmetry in the enzyme, possibly caused by intermolecular forces in the crystal, that might also influence the binding of ATP and CTP to the enzyme in the crystal. Shown in Figure 9 are schematic drawings of the helices in the allosteric domains in the T_{pam} and $R_{pam,mal}$ structures. The axes of the helices in the allosteric domains of both structures are approximately contained in the same plane. If we project the helices onto this common plane, then the axis of the H2′ helix in the R6 chain of the $R_{pam,mal}$ enzyme is about 10° off the axis of the R6 H1′ helix. In the R1 chain, the angle between the helix axes is about 22°; this angle is similar to the angles between the same helices in the R1 and R6 chains. In general, the R-state structures conform to the 2-fold noncrystallographic symmetry to a greater extent

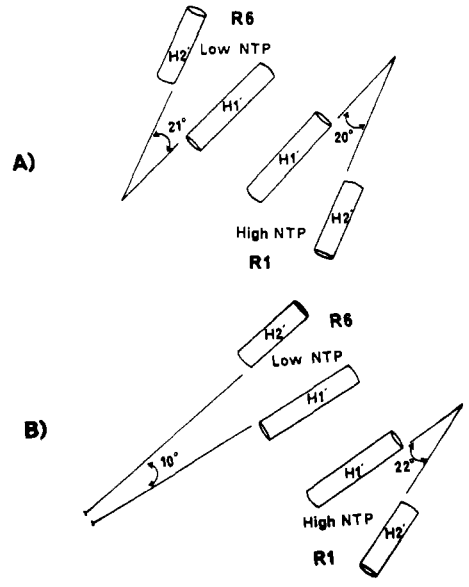

FIGURE 9: Schematic of the H1′ and H2′ helices of the allosteric domains from the T_{pam} (A) and $R_{pam,mal}$ (B) structures. Here we show a violation of the noncrystallographic symmetry in the $R_{pam,mal}$ structure. This asymmetry is also present in the R_{pala} and $R_{cp,succ}$ structures and is possibly the result of intermolecular interactions between the region of the R6 allosteric domain near residue 65 and the C-terminal portion of an adjacent molecule. In the T state, this region of the R6 allosteric domain is not involved in intermolecular contacts.

than do the T-state structures. However, the arrangement of the helices in the R6 chain of the R-state structure is clearly an exception. The cause of this breakdown in the molecular symmetry might be the intermolecular contacts between the side chains of Arg85R6 and Asp307C4; this contact is not present in the *P*321 T-state structures.

Accuracy of the Coordinates. On the basis of multiple refinements of the T_{pam} structure starting from different sets of initial coordinates and from superposition of polypeptide chains related by molecular symmetry, we estimate that error in the coordinates for which there is strong electron density, such as the residues in the active site, to be approximately 0.3 Å for the main-chain atoms and 0.5 for the side-chain atoms (Gouaux and Lipscomb, unpublished). This value is similar although slightly larger than the estimated error derived from Luzzati plots (Luzzati, 1952). If we assume that the errors in atomic positions are uncorrelated, then the error in the position of the center of a region will be smaller by a factor of $1/\sqrt{N}$ than the rms error of the individual coordinates. Since the refinement includes chemical restraints on the atoms, N is approximately 0.6 times the number of atoms included (Lesk & Chothia, 1984; Baldwin & Chothia, 1979). Therefore, the errors in the positions of large groups of atoms, such as entire domains, will be much smaller than the errors associated with individual atomic positions.

Since the small changes in the quaternary structure of the CTP-ligated enzyme could be coupled to changes in the unit cell dimensions, one must ensure that the unit cell dimensions are measured accurately. In these experiments and in other experiments performed at the same data collection facility during the same visit, the average *c*-axis unit cell dimension measured for R-state crystals in the absence of ATP or CTP is 156.5 ± 0.2 Å. Consequently, we believe that the value of 155.2 Å for the *c* cell dimension of $R^{ctp}_{pam,mal}$ crystals is significant.

As noted in other crystal structures of aspartate carbamoyltransferase, we find no density for the first seven residues in each regulatory chain. Consequently, these residues have not been included in the refinement or the analysis.

Discussion

In a previous paper (Gouaux & Lipscomb, 1990) we showed that the conformation of the R-state enzyme, as determined from crystals that were grown in the presence of PAM and malonate at pH 5.8 and subsequently transferred to a PAM and malonate buffer at pH 7.0 ($R_{pam,mal,crys}$),[2] is similar to the structure defined by X-ray data collected on crystals where the T → R transition occurred within the crystal at pH 7.0 ($R_{pam,mal,soak}$)[2]. When the $R_{pam,mal,crys}$, the $R_{pam,mal,soak}$, the $R_{cp,succ}$ (Gouaux & Lipscomb, 1988), and the R_{pala} (Ke et al., 1988) enzyme models are compared with each other, one observes that they all have very similar structures. Consequently, the $R_{pam,mal,crys}$ enzyme should be an excellent reference structure to study the effects of CTP and ATP binding.

To integrate the results of our crystallographic experiments with other studies on the heterotropic mechanism of aspartate carbamoyltransferase, we interpret much of the structural data in terms of the London and Schmidt model for the nucleotide regulation of the enzyme (London & Schmidt, 1972). Even though certain aspects of their model are wrong, such as the proposal that the bases interact directly with the Zn^{2+} ion, many of the other qualitative predictions and interpretations are correct. At a minimum, the London and Schmidt model is a good starting point for the construction of more refined models that can be based on the most recent structural and functional data. In the following discussion, we correlate previously reported experimental and theoretical data on aspartate carbamoyltransferase with our structural studies, we describe some of the differences in the regulatory dimer in the T and R states, and we speculate on how the changes induced by the binding of ATP and CTP to the $R_{pam,mal}$ enzyme might influence the contacts in the regulatory dimer that change as a consequence of the T → R transitions.

The Triphosphate Subsite. The binding site for the nucleotide triphosphates is composed of three regions: the triphosphate, the ribose, and the base subsites (London & Schmidt, 1972; Honzatko & Lipscomb, 1982a,b; Stevens et al., 1990). Our results show that the triphosphate moieties of ATP and CTP interact with their respective subsites similarly. By performing the crystallographic studies at pH 7, we find that the triphosphate groups bind more closely to the allosteric site, in contrast to the previous experiments (Honzatko & Lipscomb, 1982a,b; Kim et al., 1987; Stevens et al., 1990). The α-phosphates at pH 7 associate closely with Lys94r and the γ-phosphates bind to His20r. Arg96r is too far away to interact strongly. In ^{13}C NMR experiments on enzyme molecules specifically enriched with ^{13}C-labeled histidine residues, the three histidines in the regulatory chain responded to ATP and CTP in an identical manner (Moore & Browne, 1980). Furthermore, the histidine spectrum was undisturbed by the T → R transition (Moore & Browne, 1980), implying that the environment around His20r might not be highly sensitive to the quaternary state of the enzyme. In testing the importance of another residue in the triphosphate site, Kantrowitz and co-workers find that the Lys94r → Gln[4] mutation results in an enzyme that possesses a normal response to the

[4] The notation we use to name a mutant enzyme consists of the three-letter abbreviation of the wild-type amino acid, followed by its numerical location in the sequence on the left of an arrow and the abbreviation of the new amino acid on the right of the arrow. For example, Arg54 → Ala indicates that the arginine at position 54 was changed to an alanine.

substrates but that is almost insensitive to ATP and has a substantially reduced response to CTP (Zhang et al., 1988). The Lys94r → Gln mutant and the native enzyme exhibit similar nucleoside saturation curves in the presence of the triphosphate-truncated molecules adenosine and cytidine (Zhang et al., 1988). This result is consistent with the London and Schmidt model: the triphosphates of both ATP and CTP bind to similar residues, one of which is Lys94. Although the triphosphate subsite serves to increase the enzyme's affinity for ATP and CTP, its conformation probably does not change upon interaction with the triphosphate groups of ATP or CTP.

The Ribose Subsite. The ribose groups of ATP and CTP interact with similar residues; the 2′-hydroxyls make hydrogen bonds to the amino group of Lys60r and the 5′ oxygen is near the side chain of Asn84r. Since cytidine is nearly as effective an inhibitor as CTP and cytosine is a poor inhibitor (London & Schmidt, 1972), the binding of the ribose group to the allosteric site is important. A discussion concerning the results of changing Lys60r to an alanine residue (Zhang & Kantrowitz, 1989) is presented in Stevens et al. (1990).

The Base Subsite. The nucleoside triphosphates adopt anti conformations and the bases participate in a number of specific hydrogen bonds in a fashion similar to that proposed in general terms by London and Schmidt (1972), although they could not identify specific residues. At the allosteric site, hydrogen-bond donors arise from the NH group of Ile12r and the amino group of Lys60r; hydrogen acceptors are composed of exclusively main-chain carbonyl oxygens from Ile12r and Tyr89r. Most of the functional groups that bind to the base of ATP also interact with the pyrimidine ring of CTP, probably since the hydrogen-bonding groups on the bases are similarly disposed. The Lys60r → Ala mutant, which shows a decrease in affinity for CTP and an increase in affinity for ATP, indicates that Lys60r could play a role in the discrimination between ATP and CTP (Zhang & Kantrowitz, 1989; Stevens et al., 1990).

Upon ligation of the $R_{pam,mal}$ enzyme with ATP or CTP, the largest displacements in the protein occur in the vicinity of the bases. As predicted in the London and Schmidt model, ATP and CTP cause the base subsite to expand and contract relative to the $R_{pam,mal}$ structure, respectively. In fact, ^{19}F NMR experiments on aspartate carbamoyltransferase containing regulatory dimers with the tyrosine residues replaced by 3-fluorotyrosine residues show that ATP and CTP have different effects on the spectrum (Wacks & Schachman, 1985). It is likely that the effectors perturb the environment of Tyr89r which is located very near the base subsite. In contrast, an earlier ^{13}C NMR study employing enzyme enriched with [γ-^{13}C]Tyr did not find a perturbation of the tyrosine resonances upon ATP or CTP ligation (Moore & Browne, 1980). The discrepancy between these experiments might simply be related to the difference in the relative location of the probes. Ligation of the enzyme with ATP and CTP perturbs the environment of phenylalanine residues, as seen in the ^{13}C NMR experiments performed by Moore and Browne (1980). Interestingly, ^{13}C NMR studies of aspartate carbamoyltransferase enriched with ^{13}C-labeled phenylalanine in the regulatory chain showed that two phenylalanine residues were sensitive to CTP but not ATP binding (Moore & Browne, 1980). A candidate for one of the phenylalanines is Phe65r, the closest phenylalanine to the allosteric site, approximately 10 Å distant. However, it is not changed in position by the binding of ATP or CTP. Nonetheless, Phe65r is near Arg14r, Arg85r, and Ile86r; Ile86r is also in contact with Ile12r, a residue that interacts directly with the bases of ATP and CTP. It is possible that the binding of CTP could selectively alter the environment around Phe65r through the pathway mentioned above or through another residue, such as Arg14r, by a mechanism that is transparent to our crystallographic study at 2.8 Å. Although much of the spectroscopic data can be readily interpreted in terms of our structures, some results will require further investigation.

Germane to the construction of allosteric mechanisms are elegant studies performed by Wild and co-workers on aspartate carbamoyltransferases from other organisms. First, the aspartate carbamoyltransferase from *Serratia marcescens* has the same subunit structure as the *E. coli* enzyme and shares 88% and 77% amino acid similarities with the catalytic and the regulatory chains of the *E. coli* enzyme, respectively (Beck et al., 1989). Second, the holoenzyme from *S. marcescens* is activated by both ATP and CTP although ATP increases the enzyme's activity more than CTP (Beck et al., 1989). Third, when catalytic trimers of the *E. coli* enzyme are reconstituted with *S. marcescens* regulatory dimers, the hybrid enzyme exhibits a catalytic activity similar to that of the *E. coli* enzyme but possesses heterotropic characteristics of the *S. marcescens* enzyme (Beck et al., 1989); i.e., the hybrid is activated by both ATP and CTP. Conversely, when *S. marcescens* catalytic trimers are combined with *E. coli* regulatory dimers, this hybrid manifests the heterotropic behavior of the *E. coli* enzyme: activation by ATP and inhibition by CTP (Beck et al., 1989). Fourth, of the 33 amino acid differences in the *E. coli* and *S. marcescens* regulatory chains, there are no changes in the residues that are in direct contact with ATP or CTP based on examination of the T^{atp}, T^{ctp}, $R^{atp}_{pam,mal}$, or $R^{ctp}_{pam,mal}$ structures. Fifth, the concentration of amino acid changes is largest in the Zn domain (18 differences in 53 residues) compared to the allosteric domain (15 differences in 100 residues).

If we model the unknown structure of the *S. marcescens* regulatory dimer on the well-determined structure of the *E. coli* dimer, we can predict that the structure of the allosteric site of the *S. marcescens* enzyme is similar to that of the *E. coli* enzyme. If our crystallographic studies on the *E. coli* enzyme are true representations of the binding of effectors in solution, then the structural basis for CTP activation of the *S. marcescens* enzyme is not determined by the residues that are in direct contact with CTP; rather the ability for CTP to function as an activator is determined by residues that lie between the edge of the allosteric site and the Zn domain. Although this comparison does not tell us about the one- and three-dimensional locations of residues essential for allosteric function, it does indicate that the mechanisms by which ATP activates and CTP inhibits the *E. coli* enzyme might involve residues in the allosteric site as well as in other regions of molecule, such as the Zn···allosteric interface, for example.

Indeed, the Zn···allosteric interface undergoes substantial rearrangement as a result of the T → R transition, a transformation that has only been partially described elsewhere (Krause et al., 1987; Ke et al., 1988; Cherfils, 1987). Accompanying the T → R transition is a rotation of the regulatory dimers by 15° about the 2-fold axes, along with a significant reorientation of the zinc and allosteric domains within each regulatory chain, shown in Figures 10 and 11. This interdomain movement can be described by a rotation of ≈16° about an axis parallel to the *x*-axis, passing through the α-carbon of Arg96r of the regulatory chain (Ke et al., 1988; Cherfils, 1987). As a consequence, the packing between the first helix of the regulatory chain (H1′) and residues in the zinc domain changes. Specifically, following the superposition of the zinc domains from the T and R structures, the dis-

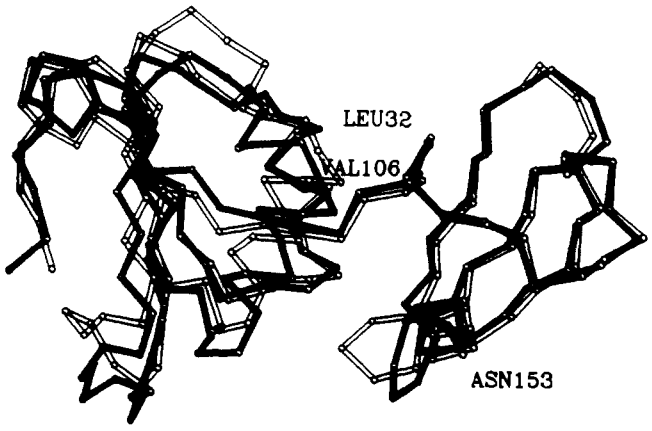

FIGURE 10: Close-up of the interface between the allosteric and zinc domains following the superposition of the α-carbons of the T_{pam} zinc domain (unfilled lines) onto the similar atoms of the $R_{pam,mal}$ structure (filled lines). Val106r and Leu32r are in van der Waals contact.

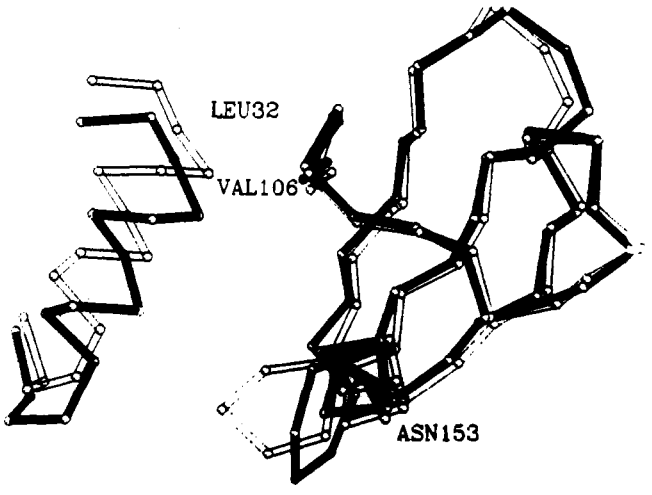

FIGURE 11: Another close-up view of the same region as in figure 10. The helix (H1′) that packs against Val106r moves approximately 2.5 Å as a result of the T to R transition. The unfilled lines represent the T_{pam} coordinates and the filled lines represent the $R_{pam,mal}$ structure.

placement between the main-chain atoms for residue Leu32r (H1′) is ≈2.5 Å. This movement occurs along the axis of the helix and alters the packing of the helix against residues in the region of Val106r in the zinc domain. In both the T and R states, the different interdigitation of the residues (31r–33r and 105r–107r) might stabilize each allosteric state and, in the absence of intermediate positions, might contribute to the two-state nature of the enzyme, in addition to the changes in hydrogen bonding pointed out earlier (Ke et al., 1988).

How then does the binding of the allosteric effectors alter the enzyme's activity? Unfortunately, neither this crystallographic study nor previous ones have exposed an obvious allosteric mechanism. Nonetheless, our studies do provide the basis for structurally plausible mechanisms. We begin with the understanding that ATP and CTP exert their strongest effects by stabilizing the R and T conformations of the regulatory dimers, respectively. Although some models for the allosteric mechanism of aspartate carbamoyltransferase postulate that ATP activation and CTP inhibition are independent of the T ⇄ R equilibrium, we have not yet determined a structural basis for such models at the current resolution of 2.8 Å; i.e., there are no significant differences in the active sites of the $R^{ctp}_{pam,mal}$ and $R^{atp}_{pam,mal}$ structures. Our conjectures are intended to stimulate further experiments designed to probe the allosteric properties of aspartate carbamoyltransferase and are not meant to imply that the proposed allosteric mechanisms are the only mechanisms that are structurally plausible.

One element of the allosteric mechanism might include interactions between the N-terminal residues of the regulatory chain, the area that undergoes the largest change upon ATP and CTP ligation. In the $R_{pam,mal}$ structures there are more interchain hydrogen bonds between the N-terminal regions compared to the T state. For example, in the R state the carboxylate of Glu10R6 makes a hydrogen bond to the NH of Val9R1 and is also near Arg41R6; in the T^{ctp} structure, Glu10R6 is only involved in a intrachain hydrogen bond to the NH group of Ala11R6. On the R1 chain in the $R_{pam,mal}$ structure, the side chain of Glu10R1, participates in a salt link with Arg41R1 which in turn interacts with Glu62R1; in the T_{pam} structure, although Arg41R1 and Glu62R1 are still bound by a salt link, the carboxylate of Glu10R1 is too far (ca. 9 Å) from Arg41R1 to interact strongly. Since an exchange of interactions between catalytic trimers and regulatory dimers for salt links and hydrogen bonds within catalytic monomers and trimers facilitates the T → R rearrangement, the R-state conformation of the regulatory dimers also might be stabilized by interchain and intrachain interactions, as typified by those involving Glu10r. ATP could stabilize the inter- and intrachain hydrogen bonds of Glu10r by increasing the size of the base subsite, pushing the R1 and R6 N-termini closer together and facilitating their interaction through residues such as Glu10r. Conversely, CTP could cause the base subsite to contract, thereby destabilizing some of the R1···R6 contacts.

The allosteric···Zn interface is another important region where the binding of ATP and CTP might be manifested, and it is an area that contributes to the stabilization of the R and T states, respectively. Specifically, a recent series of mutagenic, solution X-ray scattering and molecular mechanics (Cherfils et al., 1987), and crystallographic (Ke et al., 1988) studies indicate that an interaction between the NH_3^+ of Lys28R6 and the side chain of Asn153R6 could stabilize the R-state conformation of the regulatory dimers. On the basis of an examination of the $R_{pam,mal}$ structures, the amino group of Lys28R6 also interacts with the carbonyl oxygen of Gln24R6; the side chain of R6 Gln24 makes a hydrogen bond to Arg55R6, which also participates in a salt link to Asp39R1 and hydrogen bonds to Asn47R6. In the T_{pam} structure, Lys28r is too far from Asn153r to form a hydrogen bond, and the side chains of Gln24r and Arg55r also do not interact. This series of interactions could be one of the ways in which residues 52r–56r (50rs loop), which define portions of the triphosphate and ribose subsites, are coupled to the amino acids that define the allosteric···Zn interface. The flexibility of the 50rs loop, as determined by its elevated atomic temperature factors, is another indication that the region might mediate signal transduction. Schematic drawings showing residues that bind to CTP and ATP and possible pathways for the transduction of the allosteric information are shown in Figures 12 and 13.

ATP and CTP perturbation of the Zn···allosteric interface must be propagated to the catalytic chains through either the C1–R1 or the C1–R4 interfaces. Indeed, site-directed mutagenesis studies of enzymes that have amino acid changes at the C1–R1 interface indicate that this region is important for the heterotropic cooperativity (Xu et al., 1988). Recent crystallographic studies on the native enzyme at pH 7 (Gouaux & Lipscomb, 1990) and on the Glu239 → Gln unligated enzyme (Gouaux et al., 1989) indicate that the C1–R4 interface is critical to the stability of the T-state enzyme and is the region that could transduce the conformational changes produced by the binding of ATP and CTP. An important

CTP Ligated R State

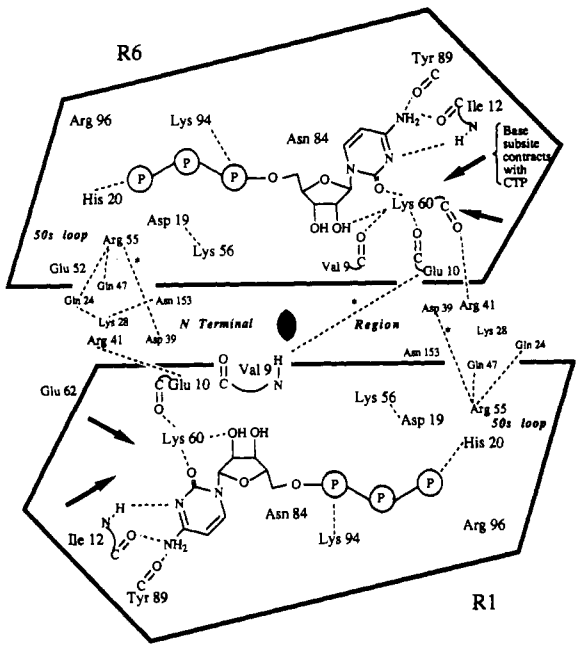

FIGURE 12: Schematic of the interactions between CTP and residues in the allosteric domains. Possible salt links and hydrogen bonds are depicted as dashed lines. Dashed lines marked with an asterisk occur between the R1 and R6 chains. Possible pathways for the transmission of allosteric information via salt links and hydrogen bonds from the allosteric site to the allosteric···Zn interface are also shown.

ATP Ligated R State

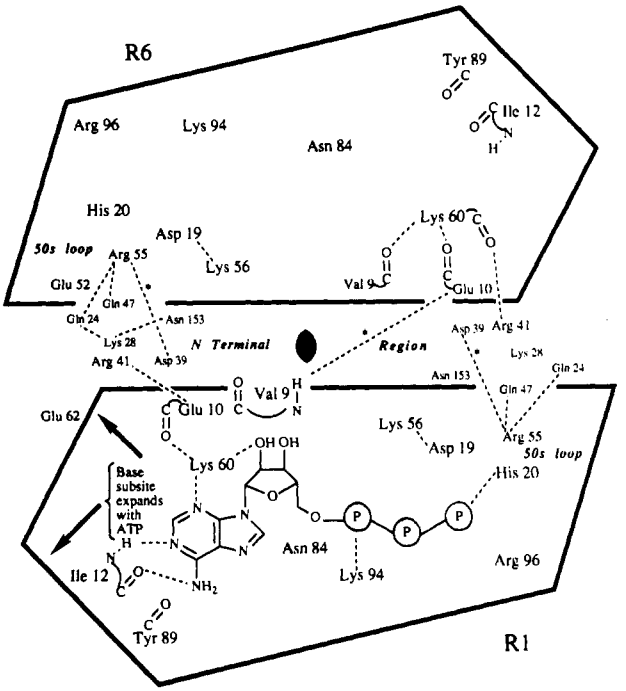

FIGURE 13: Schematic of the interactions between ATP and residues in the R1 allosteric domain. This figure is analogous to Figure 12.

interaction at the C1–R4 interface is the salt link between Asp236c and Lys143r (Gouaux et al., 1989; Gouaux & Lipscomb, 1990). The significance of this interaction was tested with site-directed mutagenesis studies, first in the experiments of Newton and Kantrowitz (1990) on the Asp236c → Ala mutant and later by Eisenstein et al. (1990) on the Lys143r → Ala enzyme. Prior to both of these studies, Cherfils et al. (1987) illustrated the importance of the C1–R4 interface in the stabilization of the T state in their study of the pAR5 mutant of aspartate carbamoyltransferase. Although experiments on mutants certainly provide a powerful method to test the function of residues in the wild-type enzyme, extrapolation of a mutant's behavior directly to the wild-type enzyme is quite possibly not as simple as some workers propound [see Eisenstein et al. (1990)]. Corder and Wild (1989) propose that "the ATP signal could be propagated through the regulatory chain into the polar domain...while the CTP signal is transmitted into the equatorial domain". However, more structural and biochemical studies will have to be carried out in order to determine whether the ATP and CTP signals follow pathways defined by a few essential residues or if the manifestation of ATP and CTP binding is dependent upon larger and more diffuse pathways that are composed of many residues.

Small changes in the packing of amino acids and not rupture or formation of hydrogen bonds and salt links probably are the mechanisms by which ligation of the $R_{pam,mal}$ enzyme with CTP decreases the separation between the upper and lower catalytic trimers by approximately 0.5 Å as seen in the $R^{ctp}_{pam,mal}$ structure. The aspartate and carbamoylphosphate domains in the catalytic chain and the zinc and allosteric domains in the regulatory chain appear to move as "rigid" bodies. This change in the average distance between the catalytic trimers could be promoted by changes in the relative disposition of the allosteric and zinc domains in the $R^{ctp}_{pam,mal}$ structure. We observe small hingelike motions between the R1–R6 allosteric domains, and also between the R6 allosteric and R6 zinc domains. These interdomain movements could result from the alterations in the allosteric binding site. For example, the side chain of Ile12r, which packs against the 10-stranded β-sheet, undergoes a substantial reorientation when CTP binds and a smaller movement upon ATP ligation. However, since these changes are small (ca. 0.5–0.8 Å), it is difficult to discern the relationship between the local and the global conformation changes with certainty. We suggest that the significance of Ile12r be tested by site-directed mutagenesis.

ATP ligation of the $R_{pam,mal}$ enzyme evokes no significant changes in the quaternary structure or in the interdomain relationships of the enzyme. As found in the analysis of the $R^{ctp}_{pam,mal}$ structure, there are also no large changes in the positions of side-chain or main-chain residues. Most significant are the small changes in the region around the purine ring, especially around Ile12R1 and Tyr89R1. The large purine ring causes the aromatic pocket to expand slightly. Possible avenues for transduction of this signal have been discussed above.

In comparing the architecture of the allosteric site to that of the active site, we observe that the binding of PAM and malonate at the active site is orchestrated by a vast array of first shell[5] hydrogen bonds and salt links that are further augmented by additional second and third shell interactions. Many of the interactions in the active site are mediated by arginine residues, the side chains of which can readily interact with a number of hydrogen-bond acceptors. In this fashion, aspartate carbamoyltransferase can form a very specific site for substrates and certain substrate analogues (Foote et al., 1985; Gouaux & Lipscomb 1990). However, the number of first shell hydrogen bonds and salt links between CTP and ATP and the allosteric site is relatively fewer, and there are

[5] In an effort to develop a more precise vocabulary for discussing the interaction between ligands and macromolecules, we will call the direct interaction between the active-site residues and PAM *first shell* interactions; the residue in question will be defined as a first shell residue. Likewise, an interaction between a residue that is not directly in contact with the ligand, but rather interacts with a *first shell* residue, will be deemed a *second shell* interaction and the residue will be called a second shell residue.

also a smaller number of second and third shell interactions, allowing the allosteric site to accommodate ligands of different size. In the allosteric site, many of the protein–effector interactions are defined by three lysines (56r, 60r, 94r), residues that cannot donate as many hydrogen bonds as arginines and residues that might allow for a more "loose" binding site. This might be one of the ways which allows the enzyme to accept both ATP and CTP in the same pocket.

ACKNOWLEDGMENTS

We thank R. H. Kretsinger, S. Sobottka, R. Chandros, and T. Ptak for the use of the Biotechnology Resource at the University of Virginia for collection of the X-ray diffraction data. We also thank Professor Kantrowitz and members of his group for assisting with the production of large quantities of enzyme and for numerous helpful discussions. We acknowledge R. Kosman, Y. M. Chook, and H. Kim for carefully reading early versions of the manuscript. We appreciate the help of Axel Brünger in setting up X-PLOR on the Cray YMP at the Pittsburgh Supercomputer Center (PSC). Use of the Cray YMP at the PSC tremendously increased the progress of this study.

REFERENCES

Allewell, N. M. (1989) *Annu. Rev. Biophys. Biophys. Chem. 18*, 71–92.

Allewell, N. M., Friedland, J., & Niekamp, K. (1975) *Biochemsitry 14*, 224–230.

Baldwin, J., & Chothia, C. (1979) *J. Mol. Biol. 129*, 175–220.

Banerjee, A., Levy, H. R., Levy, G. C., & Chan, W. W.-C. (1985) *Biochemistry 24*, 1593–1598.

Beck, D., Kedzie, K. M., & Wild, J. R. (1989) *J. Biol. Chem. 264*, 16629–16637.

Bethell, M. R., Smith, K. E., White, J. S., & Jones, M. E. (1968) *Proc. Natl. Acad. Sci. U.S.A. 60*, 1442–1449.

Brünger, A. T. (1988) *XPLOR Manual*, version 1.5, Yale University, New Haven, CT.

Buckman, T. (1970) *Biochemistry 9*, 3255–3265.

Changeux, J.-P., Gerhart, J. C., & Schachman, H. K. (1968) *Biochemistry 7*, 531–538.

Cherfils, J. (1987) Dissertation, Universite Paris-Sud, Orsay, France.

Cherfils, J., Vachette, P., Tauc, P., & Janin, J. (1987) *EMBO J. 6*, 2843–2847.

Cook, R. A., & Milne, J. A. (1977) *Can. J. Biochem. 55*, 346–358.

Corder, T. S., & Wild, J. R. (1989) *J. Biol. Chem. 264*, 7425–7430.

Eisenstein, E., Markby, D. W., & Schachman, H. K. (1990) *Biochemistry 29*, 3724–3731.

Foote, J., Lauritzen, A. M., & Lipscomb, W. N. (1985) *J. Biol. Chem. 260*, 9624–9629.

Fox, G. C., & Holmes, K. C. (1966) *Acta Crystallogr. 20*, 886–891.

Gerhart, J. C., & Pardee, A. B. (1962) *J. Biol. Chem. 237*, 891–896.

Gerhart, J. C., & Pardee, A. B. (1963) *Cold Spring Harbor Symp. Quant. Biol. 28*, 491–496.

Gerhart, J. C., & Pardee, A. B. (1964) *Fed. Proc., Fed. Am. Soc. Exp. Biol. 23*, 727–735.

Gerhart, J. C., & Schachman, H. K. (1965) *Biochemistry 4*, 1054–1062.

Gouaux, J. E., & Lipscomb, W. N. (1988) *Proc. Natl. Acad. Sci. U.S.A. 85*, 4205–4208.

Gouaux, J. E., & Lipscomb, W. N. (1989) *Biochemistry 28*, 1798–1803.

Gouaux, J. E., & Lipscomb, W. N. (1990) *Biochemistry 29*, 389–402.

Gouaux, J. E., Krause, K. L., & Lipscomb, W. N. (1987) *Biochem. Biophys. Res. Commun. 142*, 893–897.

Gouaux, J. E., Stevens, R. C., Ke, H., & Lipscomb, W. N. (1989) *Proc. Natl. Acad. Sci. U.S.A. 86*, 8212–8216.

Gray, C. W., Chamberlin, M. J., & Gray, D. M. (1973) *J. Biol. Chem. 248*, 6071–6079.

Hervé, G. (1989) in *Allosteric Enzymes* (Hervé, G., Ed.) CRC Press, Boca Raton, FL.

Hervé, G., Moody, M. F., Tauc, P., Vachette, P., & Jones, P. T. (1985) *J. Mol. Biol. 185*, 189–199.

Honzatko, R. B. (1986) *Acta Crystallogr., Sect. A 42*, 172–178.

Honzatko, R. B., & Lipscomb, W. N. (1982a) *J. Mol. Biol. 160*, 265–286.

Honzatko, R. B., & Lipscomb, W. N. (1982b) *Proc. Natl. Acad. Sci. U.S.A. 79*, 7171–7174.

Howlett, G. J., & Schachman, H. K. (1977) *Biochemistry 16*, 5077–5083.

Jones, M. E., Spector, L., & Lipmann, F. (1955) *J. Am. Chem. Soc. 77*, 819–820.

Jones, T. A. (1982) in *Computational Crystallography* (Sayre, D., Ed.) pp 303–317, Oxford, London.

Kabsch, W. (1976) *Acta Crystallogr. A32*, 922–923.

Kantrowitz, E. R., & Lipscomb, W. N. (1988) *Science 241*, 669–674.

Kantrowitz, E. R., & Lipscomb, W. N. (1990) *Trends Biochem. Sci. 15*, 53–59.

Ke, H.-M., Lipscomb, W. N., Cho, Y., & Honzatko, R. B. (1988) *J. Mol. Biol. 204*, 725–747.

Kerbiriou, D., & Hervé, G. (1973) *J. Mol. Biol. 78*, 687–702.

Kim, K. H., Pan, Z., Honzatko, R. B., Ke, H.-M., & Lipscomb, W. N. (1987) *J. Mol. Biol. 196*, 853–875.

Krause, K. L., Volz, K. W., & Lipscomb, W. N. (1987) *J. Mol. Biol. 193*, 527–553.

Ladjimi, M. M., Ghellis, C., Feller, A., Cunin, R., Glansdorff, N., Piérard, A., & Hervé, G. (1985) *J. Mol. Biol. 186*, 715–724.

Lesk, A. M., & Chothia, C. (1984) *J. Mol. Biol. 174*, 175–191.

Lipscomb, W. N., Edwards, B. F. P., Evans, D. R., & Pastra-Landris, S. C. (1975) in *Structure and Conformation of Nucleic Acids and Protein–Nucleic Acid Interactions* (Sundaralingham, M., & Rao, S. T., Eds.) pp 333–350, University Park Press, Baltimore, MD.

London, R. E., & Schmidt, P. G. (1972) *Biochemistry 11*, 3136–3142.

London, R. E., & Schmidt, P. G. (1974) *Biochemistry 13*, 1170–1179.

Luzzati, V. (1952) *Acta Crystallogr. 5*, 802–810.

Matsumoto, S., & Hammes, G. G. (1973) *Biochemistry 12*, 1388–1394.

Monaco, H. L., Crawford, J. L., & Lipscomb, W. N. (1978) *Proc. Natl. Acad. Sci. U.S.A. 75*, 5276–5280.

Monod, J., Wyman, J., & Changeux, J.-P. (1965) *J. Mol. Biol. 12*, 88–118.

Moore, A. C., & Browne, D. T. (1980) *Biochemistry 19*, 5768–5773.

Newell, J. O., Markby, D. W., & Schachman, H. K. (1989) *J. Biol. Chem. 264*, 2476–2481.

Newton, C. J., & Kantrowitz, E. R. (1990) *Proc. Natl. Acad. Sci. U.S.A. 87*, 2309–2313.

Nowlan, S. F., & Kantrowitz, E. R. (1985) *J. Biol. Chem. 260*, 14712–14716.

Pastra-Landis, S. C., Evans, D. R., & Lipscomb, W. N. (1978) *J. Biol. Chem. 253*, 4624-4630.
Perutz, M. F. (1989) *Q. Rev. Biophys. 22*, 139-236.
Pflugrath, J. W., Saper, M. A., & Quiocho, F. A. (1984) in *Methods and Applications in Crystallographic Computing* (Hall, S., & Ashiaka, T., Eds.) pp 404-407, Clarendon Press, Oxford, U.K.
Phillips, J. C., Bordas, J., Foote, A. M., Koch, M. H. J., & Moody, M. F. (1982) *Biochemistry 21*, 830-834.
Porter, R. W., Modebe, M. O., & Stark, G. R. (1969) *J. Biol. Chem. 244*, 1846-1859.
Reichard, P., & Hanshoff, G. (1956) *Acta Chem. Scand. 10*, 548-566.
Sabot, M., Cini, R., Haromy, T., & Sundaralingam, M. (1985) *Biochemistry 24*, 7827-7833.
Schachman, H. K. (1988) *J. Biol. Chem. 263*, 18583-18586.
Sobottka, S. E., Cornick, G. G., Kretsinger, R. H., Rains, R. G., Stephens, W. A., & Weissman, L. J. (1984) *Nucl. Instrum. Methods 220*, 575-581.
Stevens, R. C., Gouaux, J. E., & Lipscomb, W. N. (1990) *Biochemistry* (preceding paper in this issue).
Suter, P., & Rosenbusch, J. P. (1977) *J. Biol. Chem. 252*, 8136-8141.
Swenson, D., Baenziger, N. C., & Coucouvanis, D. (1978) *J. Am. Chem. Soc. 100*, 1932-1934.
Thiry, L., & Hervé, G. (1978) *J. Mol. Biol. 125*, 515-539.
Wacks, D. B., & Schachman, H. K. (1985) *J. Biol. Chem. 260*, 11651-11658.
Wild, J. R., Loughrey-Chen, S. J., & Corder, T. S. (1989) *Proc. Natl. Acad. Sci. U.S.A. 86*, 46-50.
Wiley, D. C., & Lipscomb, W. N. (1968) *Nature (London) 218*, 1119-1121.
Xu, W., Pitts, M. A., Middleton, S. A., Kelleher, K. S., & Kantrowitz, E. R. (1988) *Biochemistry 27*, 5507-5515.
Zhang, Y., & Kantrowitz, E. R. (1989) *Biochemistry 28*, 7313-7318.
Zhang, Y., Ladjimi, M. M., & Kantrowitz, E. R. (1988) *J. Biol. Chem. 263*, 1320-1324.

Absolute Action Spectrum of E-$FADH_2$ and E-$FADH_2$-MTHF Forms of *Escherichia coli* DNA Photolyase†

Gillian Payne and Aziz Sancar*
Department of Biochemistry and Biophysics, University of North Carolina School of Medicine, Chapel Hill, North Carolina 27599-7260

Received March 9, 1990; Revised Manuscript Received May 10, 1990

ABSTRACT: *Escherichia coli* DNA photolyase mediates photorepair of pyrimidine dimers occurring in UV-damaged DNA. The enzyme contains two chromophores, 1,5-dihydroflavin adenine dinucleotide ($FADH_2$) and 5,10-methenyltetrahydrofolylpolyglutamate (MTHF). To define the roles of the two chromophores in the photochemical reaction(s) resulting in DNA repair and the effect of DNA structure on the photocatalytic step, we determined the absolute action spectra of the enzyme containing only $FADH_2$ (E-$FADH_2$) or both chromophores (E-$FADH_2$-MTHF), with double- and single-stranded substrates and with substrates of different sequences in the immediate vicinity of the thymine dimer. We found that the shape of the action spectrum of E-$FADH_2$ matches that of the absorption spectrum with a quantum yield $\phi(FADH_2) = 0.69$. The action spectrum of E-$FADH_2$-MTHF is also in a fairly good agreement with the absorption spectrum with $\phi(FADH_2\text{-MTHF}) = 0.59$. From these values and from the previously established properties of the two chromophores, we propose that MTHF transfers energy to $FADH_2$ with a quantum yield of $\phi_{\epsilon T} = 0.8$ and that $^1FADH_2$ singlet transfers an electron to or from the dimer with a quantum yield $\phi_{ET} = 0.69$. The chemical nature of the chromophores did not change after several catalytic cycles. The enzyme repaired a thymine dimer in five different sequence contexts with the same efficiency. Similarly, single- and double-stranded DNAs were repaired with the same overall quantum yield.

DNA photolyases repair cyclobutane dipyrimidine dimers occurring in UV-irradiated DNA in a light-driven reaction. Photolyases isolated from *Escherichia coli* and *Saccharomyces cerevisiae* contain two chromophores (Jorns et al., 1984; Sancar et al., 1987b), $FADH_2$[1] (Sancar & Sancar, 1984) and 5,10-methenyltetrahydrofolylpolyglutamate (MTHF) (Johnson et al., 1988). The $FADH_2$ cofactor of the *E. coli* enzyme becomes oxidized to the neutral blue radical ($FADH^0$) during purification (Payne et al., 1987). Similarly, the MTHF cofactor is gradually lost during various stages of purification. Therefore, *E. coli* photolyase preparations contain variable amounts of MTHF in addition to the catalytically inert $FADH^0$ (Payne et al., 1987). Because of these experimental artifacts, it has been difficult to assign specific roles to each chromophore and to define their mechanisms of action in the ultimate photochemical repair process.

Action spectrum measurements by Sancar et al. (1987a) with photolyase in the form in which it is purified (containing stoichiometric $FADH^0$ and 20-50% MTHF) revealed some

†This work was supported by NIH Grant GM31082.

[1] Abbreviations: $FADH_2$, 1,5-dihydroflavin adenine dinucleotide; $FADH^0$, neutral blue radical flavin adenine dinucleotide; MTHF, 5,10-methenyltetrahydrofolylpolyglutamate; T4 endo V, T4 phage endonuclease V (UV endonuclease); EDTA, ethylenediaminetetraacetic acid; DTT, dithiothreitol; ET, electron transfer; ϵT, energy transfer; ϵ, molar extinction coefficient; ϕ, quantum yield; T<>T, cyclobutane thymine dimer; bp, base pair.

0006-2960/90/0429-7715$02.50/0 © 1990 American Chemical Society